J. Fluid Mech. (2001), *vol.* 440, *pp.* 359–380. Printed in the United Kingdom

© 2001 Cambridge University Press

Two-dimensional viscous gravity currents flowing over a deep porous medium

By JAMES M. ACTON, HERBERT E. HUPPERT AND M. GRAE WORSTER

Institute of Theoretical Geophysics, Department of Applied Mathematics and Theoretical Physics, University of Cambridge, Silver Street, Cambridge CB3 9EW, UK

(Received 24 April 2000 and in revised form 7 December 2000)

The spreading of a two-dimensional, viscous gravity current propagating over and draining into a deep porous substrate is considered both theoretically and experimentally. We first determine analytically the rate of drainage of a one-dimensional layer of fluid into a porous bed and find that the theoretical predictions for the downward rate of migration of the fluid front are in excellent agreement with our laboratory experiments. The experiments suggest a rapid and simple technique for the determination of the permeability of a porous medium. We then combine the relationships for the drainage of liquid from the current through the underlying medium with a formalism for its forward motion driven by the pressure gradient arising from the slope of its free surface. For the situation in which the volume of fluid V fed to the current increases at a rate proportional to t^3, where t is the time since its initiation, the shape of the current takes a self-similar form for all time and its length is proportional to t^2. When the volume increases less rapidly, in particular for a constant volume, the front of the gravity current comes to rest in finite time as the effects of fluid drainage into the underlying porous medium become dominant. In this case, the runout length is independent of the coefficient of viscosity of the current, which sets the time scale of the motion. We present numerical solutions of the governing partial differential equations for the constant-volume case and find good agreement with our experimental data obtained from the flow of glycerine over a deep layer of spherical beads in air.

1. Introduction

Gravity currents occur whenever fluid of one density propagates primarily horizontally into fluid of a different density. In many natural and industrial situations the intruding fluid flows over an impermeable boundary, but interesting examples also exist of gravity currents intruding into the interior of a fluid. (These examples also include the special case of a current flowing along a free surface.) A comprehensive description of many of these situations and the theory behind analysing them is presented in Simpson (1977).

The flow of relatively heavy fluid below less-dense fluid lying on a *permeable* boundary is also of natural and industrial importance but has received as yet very little attention. The additional concept introduced by this situation is that fluid can escape from the gravity current, thereby reducing its volume, as the current propagates over the permeable boundary. This situation was first considered by Thomas, Marino & Linden (1998) who, motivated mainly by industrial concerns, carried out an

https://doi.org/10.1017/S0022112001004700 Published online by Cambridge University Press

experimental investigation of a high Reynolds number salt-water gravity current in a two-dimensional channel propagating over a wire gauze into fresh water. They provided a theoretical framework to describe the results of their experiments, which incorporated the idea that the vertical velocity into the gauze at the base of the current is directly proportional to the thickness of the current at that point. This framework was further developed by Ungarish & Huppert (2000) to provide better agreement between the theoretical predictions and the experimental results of Thomas *et al.* (1998).

The aim of the present paper is to consider the propagation at low Reynolds number of a gravity current over a deep, porous substrate, which we model experimentally by a layer of spherical glass balls. In order to determine the appropriate relationship for the vertical velocity into the porous medium, we first consider the one-dimensional, purely vertical, percolation of a layer of fluid into a porous substrate. We then use the relationship obtained for the drainage velocity in terms of the thickness of the current above the porous medium and that of the fluid which has already seeped into it to investigate theoretically the two-dimensional propagation of a viscous fluid above an unsaturated (initially air-filled) porous medium.

We analyse the one-dimensional percolation in the next section and show that the fluid layer above the porous medium, which has a (hydrostatic) pressure which increases linearly with depth, drains into the porous medium in which the pressure, predicted by Darcy's Law, *decreases* linearly with depth. We describe our experimental investigations of this situation in § 3 and find good agreement between our theoretical predictions and experimental results. A consequence of this good agreement, which is dependent on the value of the permeability of the porous medium, is that we suggest a new, rapid and simple way of measuring permeabilities. We present the theoretical development for the two-dimensional propagation of a viscous gravity current over a deep permeable base in § 4. The current propagates under a balance of buoyancy and viscous forces in addition to the drainage at the base. The paradigm situation without drainage was first determined by Huppert (1982). We extend his use of lubrication theory to analyse the flow with drainage, which can be completed without the use of any experimentally determined free parameters. For the situation in which the volume input into the gravity current is proportional to t^3, where t is the time since its initiation, the governing partial differential equaions admit a similarity solution, which we obtain by numerical integration of the resulting ordinary differential equations in § 5. We then determine numerical solutions to the more general, singular, nonlinear partial differential equations in § 6 and describe our experiments in § 7. Again there is good agreement between our experimental data and the theoretical rate of propagation of the current. We summarize the work in the final section.

Our experimental setup is reproduced in millions of homes throughout the world every morning – albeit in an (approximately) axisymmetric geometry – when honey is allowed to spread out over, and seep into, freshly made toast. Other more important examples include the flow of crude oil over a beach, the propagation of a river due to tidal motions over fresh sand, and the flow of newly erupted lava over fractured bedrock.

2. One-dimensional percolation: theory

The general problem of fluid draining vertically into a porous medium is formulated in Bear (1988, p. 303), and is analysed in detail here for the case of a fixed-volume release. Consider a layer of fluid with initial height h_0 above a deep, dry, porous

https://doi.org/10.1017/S0022112001004700 Published online by Cambridge University Press

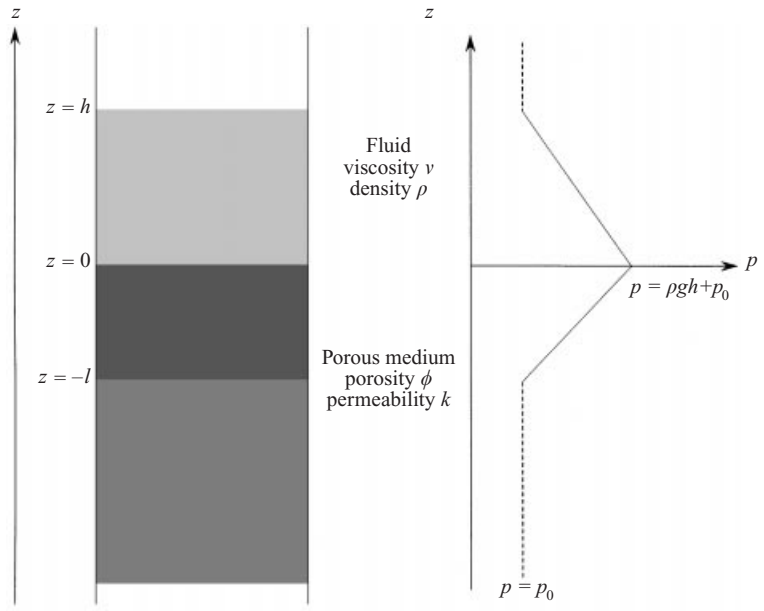


FIGURE 1. A sketch of the flow geometry and associated pressure field for the one-dimensional percolation of a layer of fluid through a deep porous medium.

medium of uniform porosity ϕ and permeability k. As sketched in figure 1, the fluid layer drains through the porous medium in such a way that after a time t it extends from $z = -l(t) < 0$ in the porous medium to $z = h(t)$ with respect to a vertical z coordinate whose origin is at the top of the porous medium. The downward volume fluxes in the fluid layer and the porous medium are independent of z (by conservation of mass) and functions only of time. In the fluid layer the pressure $p(z,t)$ can be assumed to be hydrostatic and hence given by the linear relationship

$$p(z,t) = p_0 + \rho g(h - z) \quad (0 < z < h), \tag{2.1}$$

where p_0 is the atmospheric pressure at the top of the layer, ρ is the density of the fluid and g the acceleration due to gravity.

The pressure distribution in the porous medium satisfies

$$\frac{\partial^2 p}{\partial z^2} = 0 \tag{2.2}$$

along with the boundary conditions

$$p = p_0 + \rho g h \quad (z = 0) \qquad \text{and} \qquad p = p_0 \quad (z = -l(t)), \tag{2.3a,b}$$

where the latter is a consequence of the dry portion of the porous medium being at atmospheric pressure p_0.

Surface tension acting at the base of the saturated portion of the porous medium causes the pressure there to deviate from atmospheric pressure by $\rho g h_r$, where h_r is the capillary rise height of the fluid in the porous medium. Note that h_r can be positive or negative depending on whether the fluid wets the porous medium or not. Its magnitude is less than γ/a, where γ is the magnitude of the surface tension and a is the effective radius of the pores. An estimate of the relative magnitude of the contribution of surface tension to the pressure compared with the hydrostatic presure

https://doi.org/10.1017/S0022112001004700 Published online by Cambridge University Press

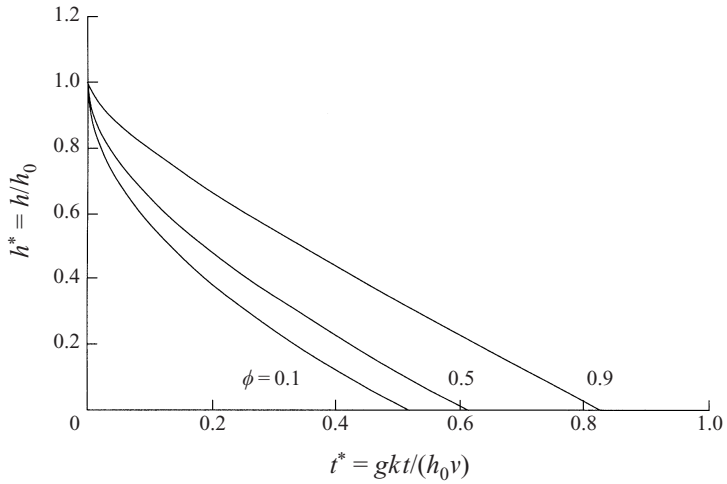


FIGURE 2. The non-dimensional height of the fluid layer percolating through a deep porous medium as a function of the non-dimensional time for various values of the porosity ϕ.

is $h_0/h_r \approx \rho g h_0 a/\gamma$, where h_0 is the initial height of the fluid layer. Therefore, surface tension can safely be neglected provided $h_0 \gg \gamma/\rho g a \approx 5\,\text{mm}$ in our experiments (see § 3 below). By way of contrast, Washburn (1921) identifies the difficulties associated with dynamic capillary rise, though the paper is spoilt by the inclusion in some parts of a slip condition at a rigid wall. More modern discussions of the problem can be found in Delker, Pengra & Wong (1996) and Davis & Hocking (2000).

From (2.2) and (2.3) it follows that the pressure distribution in the porous medium is linear and given by

$$p(z,t) = p_0 + \rho g h(1 + z/l), \tag{2.4}$$

as sketched in figure 1.

Within the porous medium the flow is governed by Darcy's law

$$\frac{\mu v}{k} = -\frac{\partial p}{\partial z} - \rho g, \tag{2.5}$$

where μ is the dynamic viscosity of the fluid and v is the transport or Darcy velocity, which is the volume flux of fluid per unit area of porous medium transverse to the flow. Differentiating (2.4) with respect to z and substituting the result into (2.5), we find that

$$v = -(gk/\nu)(1 + h/l), \tag{2.6}$$

where the kinematic viscosity $\nu = \mu/\rho$, as cited in Bear (1988). Global conservation of fluid, while $h > 0$, links h and l through

$$h + \phi l = h_0. \tag{2.7}$$

Using (2.7) to eliminate l from (2.6) and equating v to $\mathrm{d}h/\mathrm{d}t$, we find that

$$\frac{\mathrm{d}h}{\mathrm{d}t} = -(gk/\nu)\left[\frac{h_0 - (1-\phi)h}{h_0 - h}\right] \quad (h \geqslant 0) \tag{2.8a}$$

$$h(0) = h_0, \tag{2.8b}$$

https://doi.org/10.1017/S0022112001004700 Published online by Cambridge University Press

which has solution

$$t = \frac{v}{(1-\phi)gk}\left[(h_0 - h) - \frac{\phi h_0}{1-\phi}\ln\left(1 + \frac{1-\phi}{\phi h_0}(h_0 - h)\right)\right]. \tag{2.9}$$

This relationship is plotted in terms of the dimensionless variables

$$h^* = h/h_0 \qquad \text{and} \qquad t^* = gkt/(h_0 v) \tag{2.10}$$

in figure 2 for various values of ϕ. Alternatively, using (2.7), we can obtain a relationship for $l(t)$ as

$$t = \frac{v\phi}{(1-\phi)gk}\left[l - \frac{h_0}{1-\phi}\ln\left(1 + \frac{1-\phi}{h_0}l\right)\right]. \tag{2.11}$$

Expanding the logarithmic term in (2.9) for $h \approx h_0$, we find that

$$h^* = 1 - (2\phi t^*)^{1/2} + O(t^*) \qquad (t^* \ll 1). \tag{2.12}$$

Defining t_0^* as the dimensionless time when the layer of fluid has just drained ($h = 0$), we find that

$$t_0^* = \left(1 + \frac{\phi}{1-\phi}\ln\phi\right)/(1-\phi). \tag{2.13}$$

For $t^* > t_0^*$ the entire fluid lies within the porous medium, the pressure is uniform and hence the drainage velocity is a constant, which can be evaluated from (2.5) as equal to $-kg/v$.

An alternative model of drainage into a porous medium (Thomas *et al.* 1998; Ungarish & Huppert 2000) assumes that the drainage velocity into a porous medium due to an overlying fluid layer of depth h can be expressed by

$$v = -h/\tau, \tag{2.14}$$

where τ is some suitable time scale. For this drainage law, which is appropriate for drainage through a sieve rather than an extended porous medium,

$$h = h_0 \mathrm{e}^{-(t/\tau)} \tag{2.15}$$

and so, in contrast, the layer never totally drains.

Our model can be simply extended to consider the case when $h(t)$ is a given function of time, corresponding to a situation in which fluid is added to, or removed from, the system at a specified rate, as discussed in Bear (1988). We present some results briefly here, which provide a link to the draining gravity currents we examine later in the paper. Consideration of the flux of fluid into the porous medium across the plane at $z = 0$ indicates that

$$\frac{\mathrm{d}l}{\mathrm{d}t} = -v/\phi = \frac{gk}{v}\left(1 + \frac{h}{l}\right), \tag{2.16a,b}$$

which, if $h(t)$ is prescribed, can be integrated to determine $l(t)$. Alternatively, we can differentiate with respect to time to yield a first-order differential equation for $v(t)$. For the special case in which h is held constant at h_0 we find that

$$\frac{\mathrm{d}v}{\mathrm{d}t} = -\frac{(vv + gk)^2\phi}{vgh_0kv}, \tag{2.17}$$

which has the solution

$$t^* = \phi\left[\ln\left(\frac{v^*}{v^* - 1}\right) - \frac{1}{v^* - 1}\right], \tag{2.18}$$

https://doi.org/10.1017/S0022112001004700 Published online by Cambridge University Press

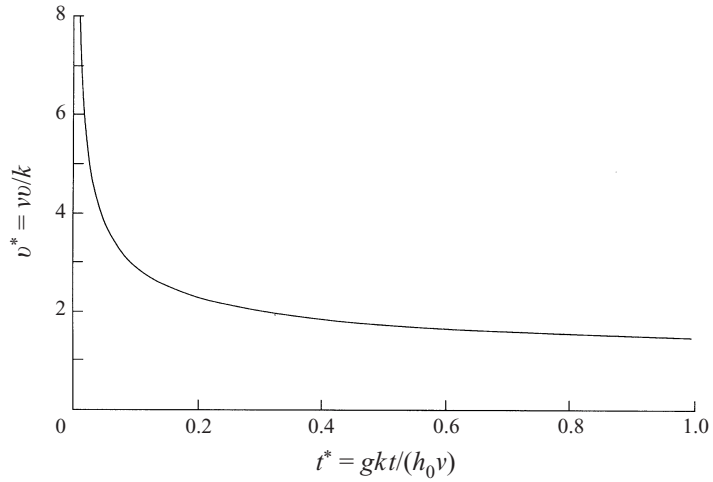


FIGURE 3. The non-dimensional velocity as a function of the non-dimensional time for a fluid layer percolating through a deep porous medium maintained at a constant height.

where

$$v^* = -vv/k. \tag{2.19}$$

The relationship (2.18) is presented in figure 3. We see that v becomes constant at large time, once $l \gg h$. We can therefore anticipate that even if a gravity current is being fed continuously, a balance might be reached between the supply of new fluid and its drainage into the underlying porous medium.

3. One-dimensional percolation: experimental confirmation

Experiments to compare with the analysis above were conducted in a Perspex tube of internal diameter 3.4 cm. The tube was filled to a depth of approximately 25 cm with spherical glass beads with a nominal diameter of 2 mm. A gauze mesh was attached to the base of the tube to hold the beads in place and to allow displaced air to escape. Four experiments were performed. For experiments 1 and 4, a volume V of glycerine, dyed with red food colouring, was poured onto the top surface of the beads as rapidly as possible from a measuring cylinder. Experiments 2 and 3 were commenced by placing a cylinder filled with glycerine above the tube containing the beads. At the base of the cylinder there was a cork which was dislodged to start each experiment. In all experiments, h and l were measured at regular time intervals by marking onto the tube the position of the relevant interfaces and then measuring those distances at the end of the experiment.

The viscosity of the glycerine was measured using a standard U-tube viscometer. The viscosity of each sample of glycerine was measured at four or five temperatures over a range of about 4 °C. A best fit exponential curve was then fitted to these data. The fit was extremely good. From this curve the viscosity of the glycerine at the temperature of the experiment, θ, was calculated. Table 1 summarizes the parameters in each of the experiments.

The porosity of the beads was measured directly. A known volume, $227\,\mathrm{cm}^3 \pm 7\,\mathrm{cm}^3$ (corresponding to a tube length of $25.0\,\mathrm{cm} \pm 0.2\,\mathrm{cm}$) was sealed at one end and filled with beads. Water was then poured into the tube to just fill the pore spaces. We found that $83\,\mathrm{cm}^3 \pm 3\,\mathrm{cm}^3$ was required. Hence ϕ was calculated as 0.37 ± 0.02.

https://doi.org/10.1017/S0022112001004700 Published online by Cambridge University Press

Quantity	Experiment 1	Experiment 2	Experiment 3	Experiment 4
θ (°C)	21.5 ± 0.1	22.4 ± 0.1	21.2 ± 0.1	21.9 ± 0.1
V (cm^3)	80 ± 3	72.8 ± 0.2	88.4 ± 0.2	67.8 ± 1
L (cm)	25.1 ± 0.3	23.6 ± 0.3	25.8 ± 0.3	25.2 ± 0.3
h_0 (cm)	8.8 ± 0.4	8.0 ± 0.2	9.7 ± 0.3	7.5 ± 0.2
v (cm^2 s^{-1})	9.75 ± 0.1	9.07 ± 0.1	9.12 ± 0.1	9.06 ± 0.1

TABLE 1. Parameter values for the one-dimensional percolation experiments.

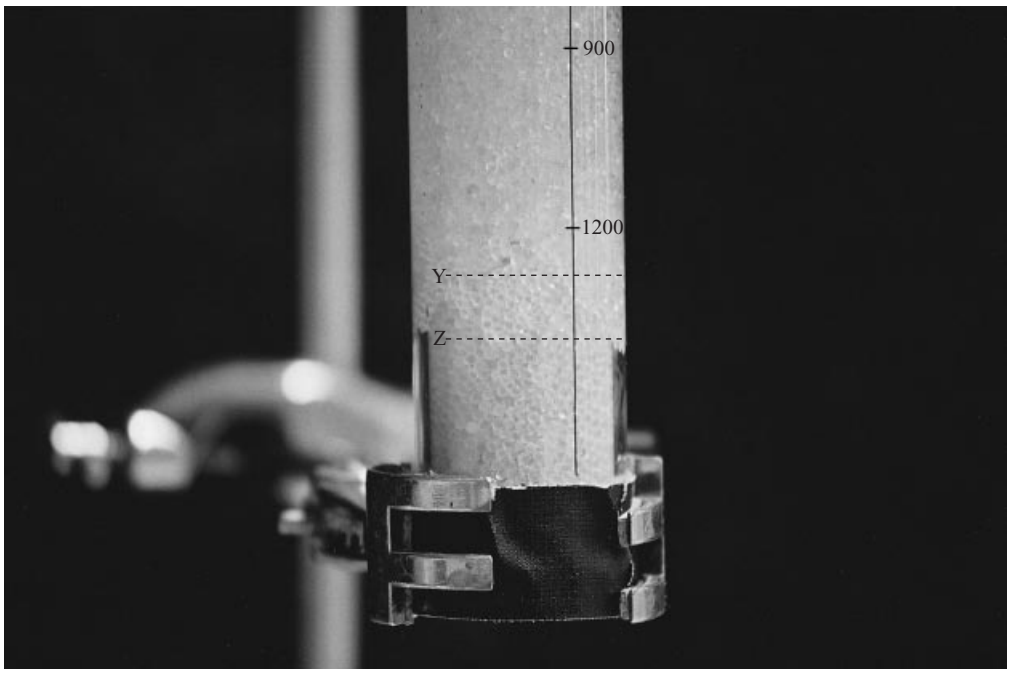


FIGURE 4. A photograph of experiment 4 near the base of the percolating fluid medium showing the two extreme interface positions.

Figure 4 shows a photograph of the interface at $z = -l$, fifteen minutes after commencement of a typical experiment. Two features are evident. First there is not a sharp transition between fluid and beads, but between the lines Y and Z there is a slightly paler region of fluid. This occurred because the interface at Y was subject to the usual Rayleigh–Taylor instability (Phillips 1991). In addition, the beads do not pack around the edge of the tube as efficiently as they do in the centre; there is a region of higher porosity and permeability around the edge. Hence fluid can flow faster along the edges of the tube than it can down the centre. This would result in fluid being present throughout the cross-section of the tube above Y, but between Y and Z it would be present only around the edges, thereby accounting for the paler region. In experiments 1 and 2 we took the position of the interface at Z while in experiments 3 and 4 we took Y as the position for the interface. As we show below it made little difference to the results.

The error in time measurement is about ± 0.5 s. The dominant cause of error in the measurement of l is the uncertainty in the position of the interface, with an

https://doi.org/10.1017/S0022112001004700 Published online by Cambridge University Press

	h_1	l_1	h_2	l_2	h_3	l_3	h_4	l_4	Ave.	Std. dev.
ϕ	0.284	0.434	0.468	0.396	0.371	0.285	0.319	0.218	0.35	0.3
k_1 (cm$^2 \times 10^{-5}$)	3.11	4.05	2.81	3.17	3.15	2.57	2.84	1.67	2.9	0.7
k_2 (cm$^2 \times 10^{-5}$)	2.88	3.29	3.06	2.91	3.15	3.51	2.71	3.14	3.1	0.3

TABLE 2. Values for ϕ and k (labelled k_1) from a two-parameter regression and values of k (labelled k_2) from a one-parameter regression with $\phi = 0.37$ of the data for h and l otained from experiments 1–4 (indicated by subscripts).

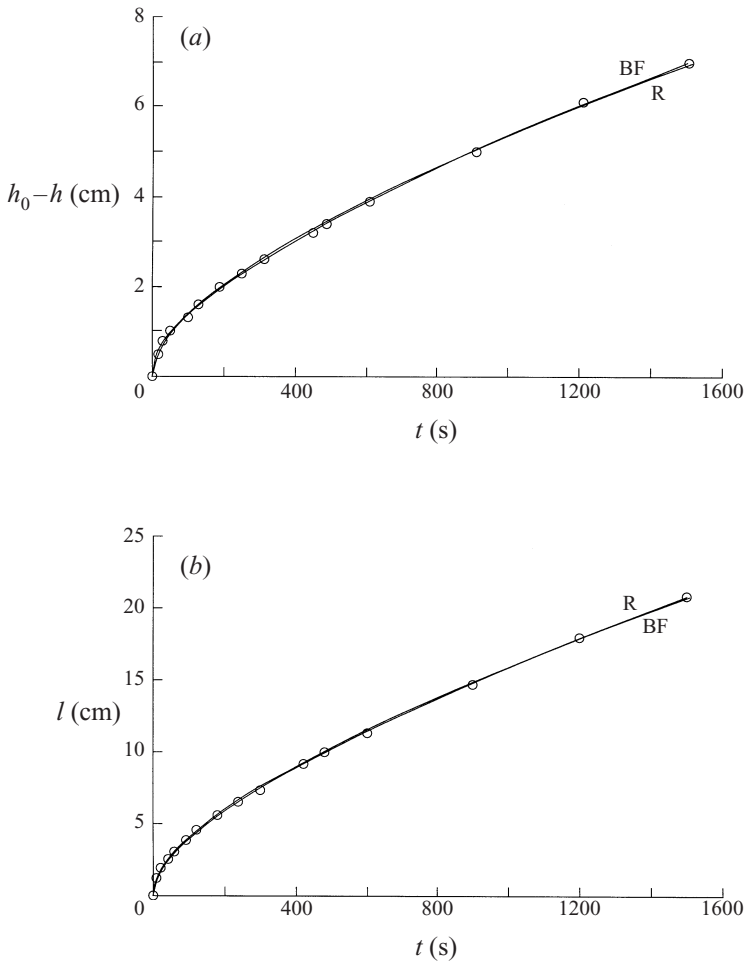


FIGURE 5. (*a*) The drainage of the fluid layer and (*b*) the depth of the fluid layer within the porous medium as functions of time for experiment 4. The circles represent experimental data. The curves marked BF represent the best-fit curves (2.9) allowing both k and ϕ to be free. The curves marked R are the best-fit curves for $\phi = 0.37$ allowing k to be free.

estimated error of about 3%. The dominant error in h of about ± 0.5 mm is simply that introduced by the actual acts of marking and measuring the position of the interface.

Figures 5(*a*) and 5(*b*) present data for h_0-h and l as functions for t for experiment 4,

https://doi.org/10.1017/S0022112001004700 Published online by Cambridge University Press

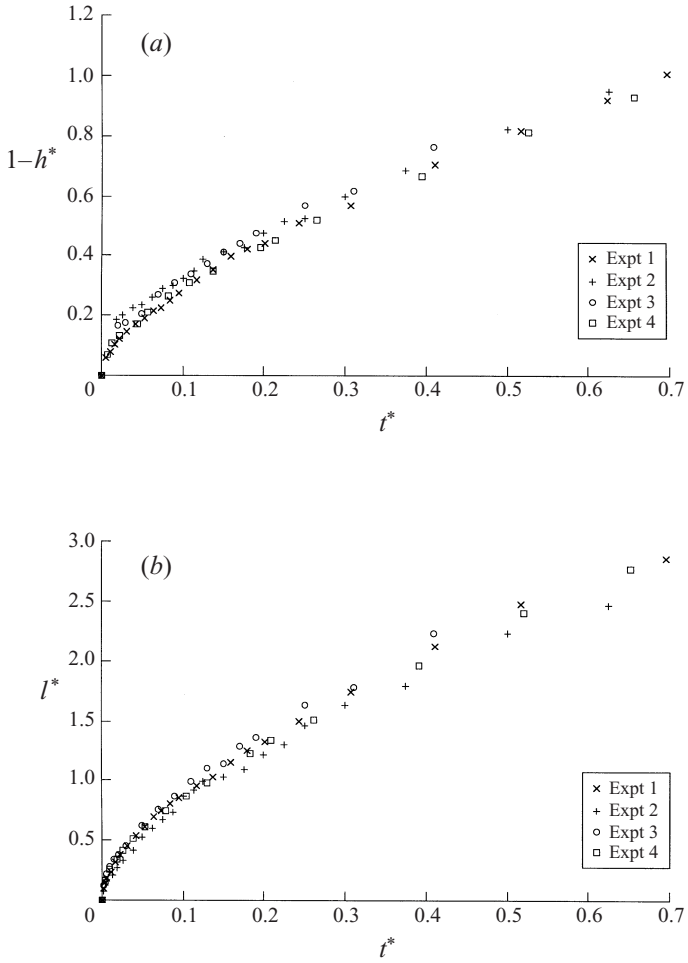


FIGURE 6. (*a*) The non-dimensional decrease in the height of the fluid layer and (*b*) the non-dimensional depth of percolation as functions of non-dimensional time for each of the four experiments.

a typical experiment. We determined estimates for ϕ and k by finding those values for which (2.9) and (2.10) most closely followed the experimental data in a least-squares sense. The resulting best-fit curves are drawn in figures 5(*a*) and 5(*b*) and labelled BF. Table 2 shows the two values of ϕ and k estimated in this way from the data for each experiment. As can be seen from the best-fit curve in the case of experiment 4 (and from all the residuals, all of which were greater than 0.998), the best-fit curves match the data very well. However, the variations in the values determined for ϕ from each experiment were rather large, even though the average of 0.35 ± 0.08 was close to the directly measured value of 0.37. Consequently a second series of curves was fitted in which ϕ was specified as 0.37 and the error minimized with respect to k only. The mean values of k and the standard deviations are shown in the final columns of table 2. The new set of best-fit curves for experiment 4 are shown in figures 5(*a*) and 5(*b*) and marked R.

From the curves it is clear that there is little difference between the first set and the second. This indicates that the curves are rather insensitive to changes in ϕ and

https://doi.org/10.1017/S0022112001004700 Published online by Cambridge University Press

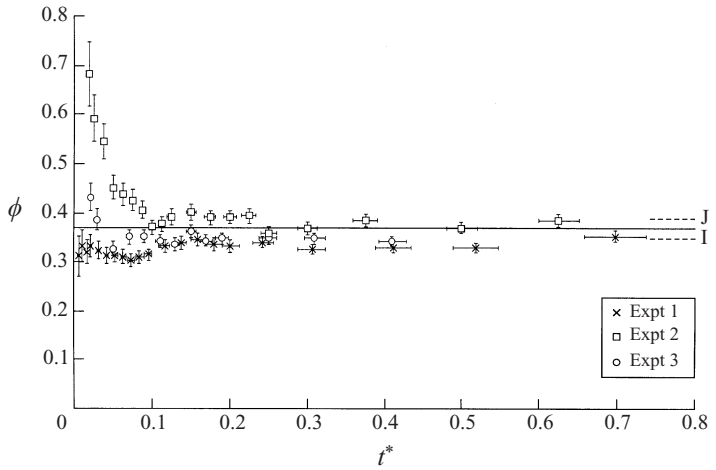


FIGURE 7. The experimentally determined porosity, evaluated from $\phi = (h_0 - h/l)$, as a function of non-dimensional time for the first three experiments. The dashed lines I and J indicate one standard deviation on either side of the mean.

hence that estimates of ϕ from the curves are not likely to be accurate. Note that for the first two experiments, for which measurements were taken at the top of the paler region, the average value of k is $(3.04 \pm 0.09) \times 10^{-5}\,\mathrm{cm}^2$, while for the second pair of experiments, for which measurements were taken at the very bottom of the fluid, it is $(3.13 \pm 0.2) \times 10^{-5}\,\mathrm{cm}^2$. These values are not significantly different. We therefore take $3.1 \times 10^{-5}\,\mathrm{cm}^2$ to be the value of the permeability determined from our experiments.

Figures 6(*a*) and 6(*b*) present plots of $1 - h^*$ and $l^* = l/h_0$ against t^* for the data from all our experiments along with (2.9) and (2.11) using $\phi = 0.37$ and $k = 3.1 \times 10^{-5}\,\mathrm{cm}^2$. The data are seen to collapse very well. (Error bars have not been shown on these plots for the sake of clarity but they are certainly large enough to explain any variations between experiments.)

A number of empirical relationships connecting k and ϕ have been suggested. One of the simplest and most frequently used is the Carman–Kozeny equation (Dullien 1979; Phillips 1991)

$$k = \frac{D^2\phi^3}{180(1-\phi)^2}, \tag{3.1}$$

where D is the mean diameter of the particles in the porous medium. The diameter of 30 balls was measured using vernier callipers and the mean diameter found to be $0.204 \pm 0.003\,\mathrm{cm}$. Taking $\phi = 0.37 \pm 0.02$ gives an estimate, using the Carman–Kozeny equation, of $k = 3.0 \pm 0.5 \times 10^{-5}\,\mathrm{cm}^2$, which is in good agreement with our direct experimental measurements. Another relationship, originally proposed by Rumpf & Gupte (1971) and reviewed in Dullien (1979), for randomly packed spheres with porosities between 0.35 and 0.65 is given by

$$k = \frac{1}{5.6} D^2 \phi^{5.5}. \tag{3.2}$$

With the values indicated above, this leads to a mean value of k of 3.1×10^{-5}, not dissimilar to that obtained from using (3.1).

A different estimate of ϕ can be obtained using (2.7). The ratio $(h_0 - h)/l$ should equal ϕ and figure 7 shows a plot of $(h_0 - h)/l$ against t^* for each of the first three

https://doi.org/10.1017/S0022112001004700 Published online by Cambridge University Press

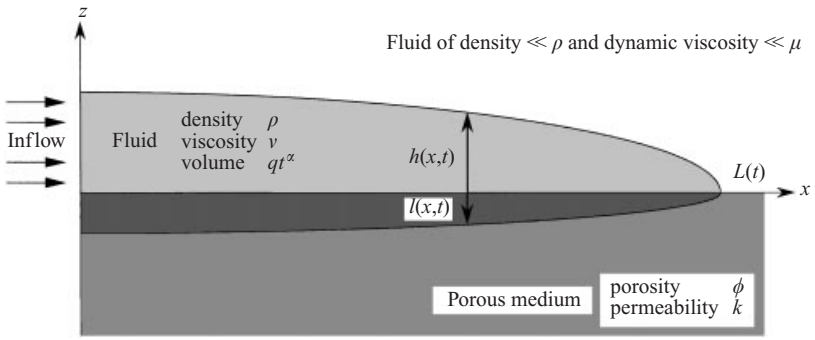


FIGURE 8. A sketch of the coordinate system used to evaluate the flow of a two-dimensional gravity current over a deep porous medium.

experiments. (For experiment 4, h and l were measured at different times, preventing such an estimate.) Except at early times ($t^* < 0.1$), the deduced values of ϕ become reasonably constant and consistent with the previously estimated value of 0.37 ± 0.02. At early times there are deviations from this, especially with experiment 2. This is not surprising however, since at early times the values of $h_0 - h$ and l are small, and hence difficult to measure accurately, as well as being considerably influenced by the way in which the experiment was started. Releasing fluid in the way it was for experiment 2 will certainly not lead to the idealized situation of the entire head of fluid resting on the interface at $t = 0$. This is reflected in figure 7 where the experimental data deviate most markedly at early times.

4. Advection plus drainage: theory

We consider now the two-dimensional flow of a viscous gravity current over a deep porous medium, as sketched in figure 8. In addition to the horizontal advection of fluid above the porous medium, there is also vertical drainage into the underlying medium. With the approximations of lubrication theory (Batchelor 1967) which are valid once the horizontal length becomes very much greater than the vertical thickness, the velocity profiles for the vertical and horizontal flows can be derived independently. They are then interrelated by the fact that the drainage, which is dependent on the local thickness of the current above the porous medium, reduces the thickness and hence changes the propagation of the current.

The horizontal velocity profile, which experiences no slip at $z = 0$ and no tangential stress at $z = h$, in the current is given by

$$u(x,z,t) = -\frac{1}{2}\left(\frac{g}{\nu}\right)\frac{\partial h}{\partial x} z(2h - z) \quad (0 \leqslant z \leqslant h). \tag{4.1}$$

From local continuity, u, h and v are related by

$$\frac{\partial h}{\partial t} + \frac{\partial}{\partial x}\left(\int_0^h u \mathrm{d}z\right) = v(x,0,t), \tag{4.2}$$

where, as discussed in § 2,

$$v(x,0,t) = -(gk/\nu)(1 + h/l) = -\phi\frac{\mathrm{d}l}{\mathrm{d}t}. \tag{4.3a,b}$$

Note that the horizontal component of flow in the porous medium, which is driven

https://doi.org/10.1017/S0022112001004700 Published online by Cambridge University Press

by the horizontal gradient of the hydrostatic pressure exerted by the overlying fluid, is $(kg/v)\partial h/\partial x$. This has magnitude much less than $v \sim kg/v$ and is therefore ignored in this analysis. Note too that surface tension at the base of the saturated region can be ignored once $(h+\phi l) \gg h_r$. We neglect its effects here but discuss them later in the context of our experimental results. Substituting (4.1) and (4.3*a*) into (4.2), we obtain

$$\frac{\partial h}{\partial t} - \frac{1}{3}\left(\frac{g}{v}\right)\frac{\partial}{\partial x}\left(h^3\frac{\partial h}{\partial x}\right) = -(kg/v)(1+h/l) \tag{4.4}$$

as a partial differential equation linking h and l in addition to (4.3*b*).

Finally, the total conservation of fluid, on the assumption the fluid is input so that the total amount is given by $V = qt^\alpha$ for some constant q and α, requires

$$\int_0^L (h+\phi l)\mathrm{d}x = qt^\alpha, \tag{4.5}$$

where $L(t)$ is the length of the current.

The relationships (4.4) and (4.5) can be reduced to those derived by Huppert (1982, 1986, 2000) for the flow of a viscous gravity current propagating over a rigid horizontal boundary by setting the right-hand side of (4.4) to zero (zero drainage velocity) and setting $\phi l = 0$ in (4.5).

Equations (4.4) and (4.5) contain five physical parameters, g, v, k, q and ϕ. The first four can be eliminated from the equations leaving ϕ as the only parameter, which makes the determination and interpretation of the solutions much easier. This is done by introducing the non-dimensional quantities

$$\eta = h/S_V, \quad \zeta = l/S_V \quad X = x/S_H \qquad \text{and} \qquad T = t/S_t, \tag{4.6a–d}$$

where the vertical, horizontal and temporal scales S_V, S_H and S_t are given by

$$S_V^{6-2\alpha} = 3q^2v^{2\alpha}k^{1-2\alpha}/g^{2\alpha}, \quad S_H^{6-2\alpha} = q^4v^{4\alpha}/(3^{1-\alpha}g^{4\alpha}k^{3\alpha+1}), \quad S_t^{6-2\alpha} = 3v^6q^2/(g^6k^5). \tag{4.7a–c}$$

Substituting (4.6) and (4.7) into (4.3*b*), (4.4) and (4.5), we obtain

$$\frac{\partial \eta}{\partial T} - \frac{\partial}{\partial X}\left(\eta^3\frac{\partial \eta}{\partial X}\right) = -\left(\frac{\eta+\zeta}{\zeta}\right), \tag{4.8}$$

$$\frac{\partial \zeta}{\partial T} = \left(\frac{\eta+\zeta}{\phi\zeta}\right), \tag{4.9}$$

and

$$\int_0^{X_N} (\eta+\phi\zeta)\mathrm{d}X = T^\alpha, \tag{4.10}$$

as the governing equations in dimensionless form, where the dimensionless front of the current $X_N = L/S_H$.

The associated boundary conditions are

$$\eta = \zeta = 0, \quad \eta^3\frac{\partial \eta}{\partial X} \to 0 \quad (X = X_N). \tag{4.11a–c}$$

The third of these boundary conditions is a statement of conservation of mass at the nose of the current: that there is no sink of fluid there.

We note that the scalings (4.7) become undefined at $\alpha = 3$, a significant value, as we shall show below. Only for $\alpha = 3$ does (4.8)–(4.10) have a similarity solution for

https://doi.org/10.1017/S0022112001004700 Published online by Cambridge University Press

which effects due to spreading, as expressed by the second term on the left-hand side of (4.8), continually balance effects due to drainage, as expressed by the term on the right-hand side.

At early times, the dominant balance in equation (4.8) when $\alpha < 3$ is between the terms on its left-hand side, and $\eta \gg \zeta$, which gives the asymptotic scalings

$$\eta \sim T^{(2\alpha-1)/5}, \quad X_N \sim T^{(3\alpha+1)/5}, \quad \zeta \sim T^{(\alpha+2)/5}, \quad t \ll 1. \tag{4.12}$$

This can be verified by direct substitution, which shows that although the drainage term on the right-hand side of (4.8) is singular as $t \to 0$, being proportional to $T^{-(3-\alpha)/5}$, the terms on the left-hand side are more singular, being proportional to $T^{-2(3-\alpha)/5}$. This means that, for $\alpha < 3$, the dynamics of the gravity current are dominated by spreading at early times and the solutions are asymptotic to the non-draining similarity solutions calculated by Huppert (1982).

In particular, for $\alpha = 0$, the entire right-hand side of (4.8) is negligible as $t \to 0$, and ζ is negligible compared with η on the right-hand side of (4.9) and in the integrand of (4.10). The solution of the resulting equations is

$$\eta \sim T^{-1/5} s_N^{2/3} \left[\tfrac{3}{10}(1 - Y^2)\right]^{1/3}, \tag{4.13}$$

$$\phi\zeta^2 \sim 5\left(\tfrac{3}{10}\right)^{1/3} T^{4/5} s_N^{2/3} Y^4 \int_{Y^2}^{1} u^{-3}(1-u)^{1/3}\mathrm{d}u, \tag{4.14}$$

where

$$X_N = s_N T^{1/5}, \quad s_N = \left[\frac{\frac{1}{5}\left(\frac{3}{10}\right)^{1/3}\pi^{1/2}\Gamma\left(\frac{1}{3}\right)}{\Gamma\left(\frac{5}{6}\right)}\right]^{-3/5} \simeq 1.411 \tag{4.15a,b}$$

and $Y = X/X_N(t)$. This provides the initial conditions for the full numerical solution described below.

At late times, when $\alpha < 3$, the second term on the left-hand side of (4.8) is negligible; the current stops spreading and simply drains into the porous medium in the manner described in §§ 2 and 3. The transition between the early spreading behaviour and the late draining behaviour occurs when $T^{3-\alpha} = O(1)$, which imples that $T = O(1)$, since $\alpha < 3$. This is equivalent to a dimensional time $t \sim S_t$. For the important case of $\alpha = 0$, this transition time is

$$t_T \sim \frac{\nu q^{1/3}}{g k^{5/6}}, \tag{4.16}$$

which increases with the viscosity and with the initial volume of the current, as might be expected.

It is also clear from these scalings that all the terms in (4.8) balance for all time when $\alpha = 3$. This unique balance gives rise to a similarity solution.

5. The similarity solution for $\alpha = 3$

By writing down order-of-magnitude expressions for each term in (4.8)–(4.10), it is straightforward to show that a similarity form of solution only exists for $\alpha = 3$. In this case a suitable similarity variable can be written as $s = X/T^2$ and corresponding relationships for η and ζ are of the form

$$\eta = T\psi(s) \qquad \text{and} \qquad \zeta = T\chi(s). \tag{5.1a,b}$$

https://doi.org/10.1017/S0022112001004700 Published online by Cambridge University Press

Substituting (5.1) into (4.8)–(4.10), we obtain

$$\psi - 2s\psi' - 3\psi^2\psi'^2 - \psi^3\psi'' = -(1 + \psi/\chi) \tag{5.2}$$

$$\chi - 2s\chi' = (1 + \psi/\chi)/\phi \tag{5.3}$$

and

$$\int_0^{s_N} (\psi + \phi\chi)\mathrm{d}s = 1, \tag{5.4}$$

where primes denote differentiation with respect to s and $s_N = X_N/T^2$, which indicates immediately that for $\alpha = 3$, L is proportional to t^2.

The equations (5.2)–(5.4) were solved numerically using the computer algebra package *Mathematica*, with the built-in numerical differential equation solver *NDSolve*. The equations were first manipulated to give the more convenient set of coupled first-order differential equations

$$y_1' = y_2, \tag{5.5a}$$

$$y_2' = (y_1 - 2sy_2 - 3y_1^2y_2^2 + 1 + y_1/y_3)/y_1^3, \tag{5.5b}$$

and

$$y_3' = \frac{1}{2s}\left(y_3 - \frac{y_1 + y_3}{\phi y_3}\right), \tag{5.5c}$$

where the variables y_1, y_2 and y_3 are related to ψ and χ by $y_1 = \psi$, $y_2 = \psi'$ and $y_3 = \chi$. A new function y_4, representing the total volume of the gravity current between the point η and its nose, at s_N, was defined as

$$y_4 = \int_s^{s_N} (y_1 + \phi y_3)\mathrm{d}s. \tag{5.6}$$

Differentiating (5.6), we obtain

$$y_4' = -(y_1 + \phi y_3) \tag{5.7}$$

as the fourth, coupled, first-order, ordinary differential equation. The appropriate boundary conditions associated with (5.5) and (5.7) are

$$y_1 = y_3 = 0, \quad y_1^3y_2 \to 0 \quad (s = s_N) \qquad \text{and} \qquad y_4 = 1 \quad (s = 0). \tag{5.8a–d}$$

In order to determine the explicit solutions to (5.5) and (5.7) it was first necessary to evaluate s_N. This was done by integrating the equations backward from $s = s_N$ to $s = 0$ with varying values of s_N until the boundary condition (5.8c) was satisfied. Because of the singularity at $s = s_N$ it was necessary to commence the integrations with the asymptotic representations, which can be derived directly from (5.5) and (5.7),

$$y_1(s) \sim [6s_N(s_N - s)]^{1/3}, \quad y_2(s) \sim -\tfrac{1}{3}(6s_N)^{1/3}(s_N - s)^{-2/3}, \tag{5.9a, b}$$

$$y_3(s) \sim \left(\frac{81}{32s_N^2\phi^3}\right)^{1/6}(s_N - s)^{2/3}, \quad y_4(s) \sim \tfrac{3}{4}(6s_N)^{1/3}(s_N - s)^{4/3} \quad (s \uparrow s_N). \tag{5.9c, d}$$

Figure 9 graphs the calculated values of s_N as a function of ϕ. Once the value of s_N has been obtained, numerical integration of (5.5) and (5.7) starting with (5.9) yields ψ and χ. Figure 10 presents a plot of ψ and χ for $\phi = 0.5$ (for which $s_N = 0.574$). For s larger than about 0.3, $\psi > \chi$ – in the forward portion the height of the current

https://doi.org/10.1017/S0022112001004700 Published online by Cambridge University Press

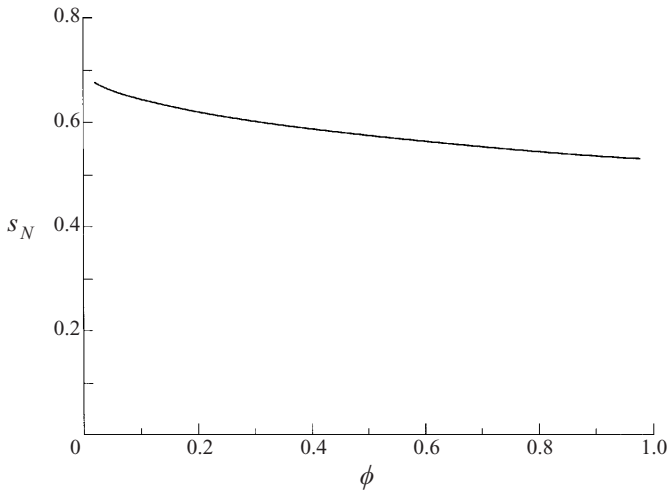


FIGURE 9. The value of s_N as a function of ϕ for $\alpha = 3$.

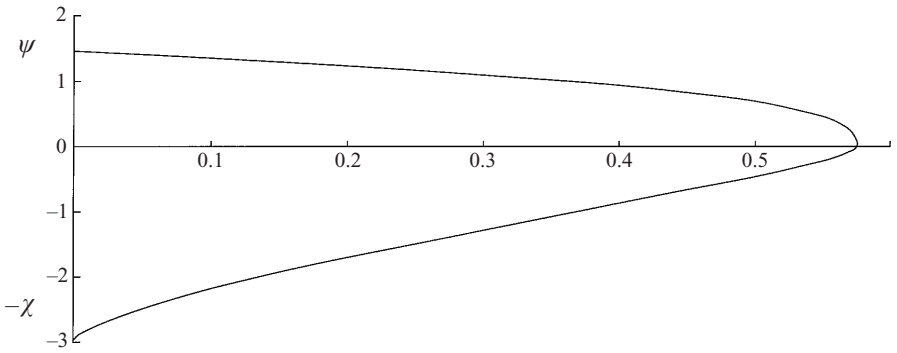


FIGURE 10. The self-similar shape of the gravity current for $\phi = 0.5$ and $\alpha = 3$.

above the bed exceeds that in the porous medium (in accord with (5.9*a*, *c*)) – while for s less than approximately 0.3 the opposite is true.

6. Numerical solutions for $\alpha = 0$

When $\alpha \neq 3$, it is necessary to solve the partial differential equations (4.8)–(4.10). There are difficulties associated with the fact that the boundary $X = X_N$, the nose of the current, is moving and that the solutions are singular there. These were overcome by first mapping the domain $[0, X_N]$ onto $[0, 1]$. The resulting equations were solved numerically using a predictor-corrector scheme with first-order convergence. The details of this procedure are described in the Appendix. Aspects of the code were tested by using it to predict the length of a non-draining gravity current, and comparing the results to the analytic solutions (Huppert 1982), and to predict the one-dimensional drainage into a porous medium described in § 2. In both cases, excellent agreement between the numerical and analytical results was obtained.

Figure 11 shows a plot of $X_{\max}$, the maximum length of the gravity current X_N, as a function of ϕ for $\alpha = 0$, as obtained from the numerical integration. In particular, $X_N = 0.858$ at $\phi = 0.37$. Figure 12 shows the evolution of the shape of a gravity

https://doi.org/10.1017/S0022112001004700 Published online by Cambridge University Press

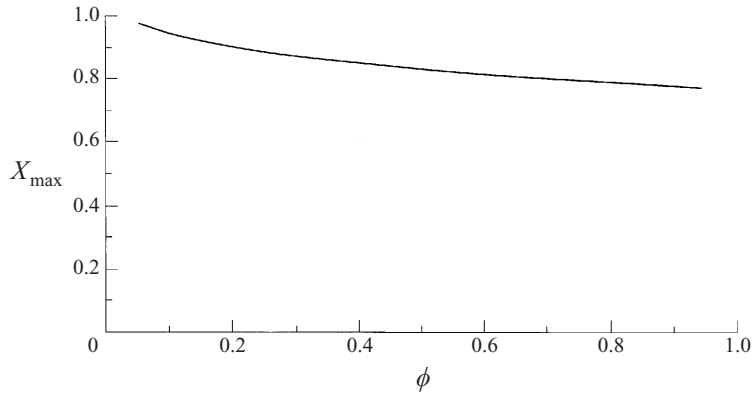


FIGURE 11. The value of $X_{\max}$ as a function of ϕ for $\alpha = 0$.

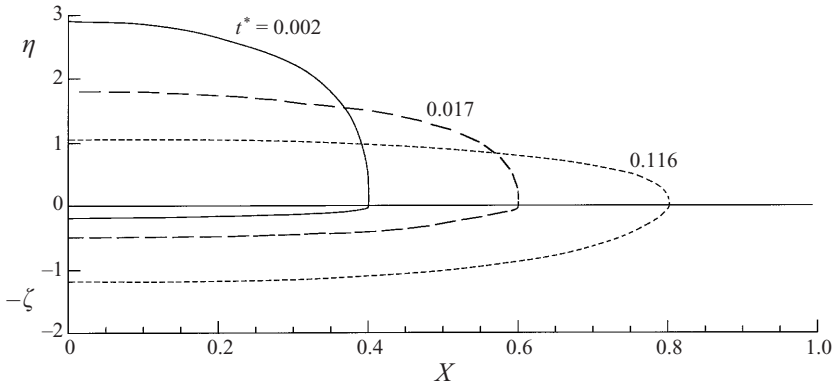


FIGURE 12. The evolution of the shape of the current for $\alpha = 0$ and $\phi = 0.37$. In the current shown at $t^* = 0.002$, when $X_N = 0.4$, spreading dominates drainage and the similarity solutions (4.13)–(4.15) give a good aproximation to the shape of the current. In the current shown at $t^* = 0.116$, when $X_N = 0.8$, the current has almost arrested and is dominated by drainage.

current of constant volume ($\alpha = 0$) for a porosity of 0.37, the porosity of the bed used in the experiments.

7. Experimental investigations

We conducted experiments in two Perspex tanks whose cross-sections are sketched in figure 13. Each tank was 15.1 cm $\pm$ 0.05 cm in width. Before the start of each experiment the region labelled B was filled with thoroughly washed and dried spherical glass beads of nominal diameter 2 mm. The bed was carefully flattened and levelled. The region labelled F, behind the lock, was filled with glycerine dyed with red food colouring. The length of the lock could be varied by the insertion of a second gate R. At $t = 0$ the gate G was raised, which allowed the gylcerine to flow from the lock onto the beads. About a second later the gate G was rapidly replaced. This procedure was carried out because the theoretical model assumes that the gravity current is entirely underlain by a porous bed and if the gate were not replaced then there would be a section of the gravity current, that part still in the lock, which is above an impermeable surface. The volume of fluid released was calculated from measurements of the height of the liquid in the lock before and after the gate was opened.

https://doi.org/10.1017/S0022112001004700 Published online by Cambridge University Press

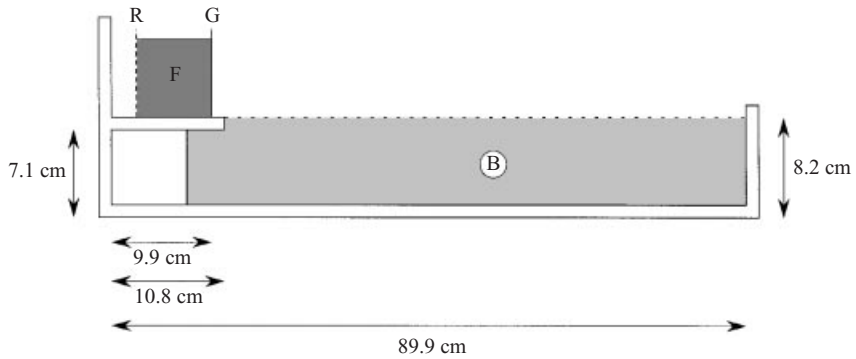


FIGURE 13. A schematic diagram of the apparatus used in the two-dimensional experiments.

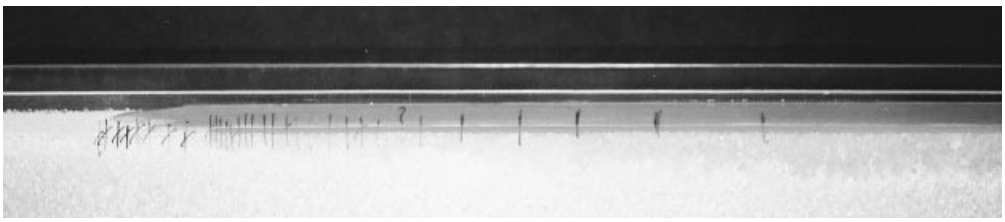


FIGURE 14. A photograph of an experiment.

At regular time intervals the length L of the gravity current from the gate G was measured by placing marks on the tank at the position of the front of the gravity current. These positions could then be measured accurately after each experiment. The front of the gravity current, as shown for a typical experiment in figure 14, was not perfectly straight but showed some irregularities. There was therefore some degree of uncertainty as to the position of the front of the gravity current. We measured the frontmost point of the leading edge but the front, across the tank, would on average have been some way behind that. This lack of two-dimensionality manifested itself predominantly in experiments with smaller volumes though the 'fringe' of the current in all the experiments was less than 5% of the total current length. The error in t reflects the difficulty of taking a measurement at exactly the right time and an estimate is ± 0.2 s.

Observations were also made of the flow within the porous medium. Finger-like Rayleigh–Taylor instabilities were seen protruding from the bottom of the flow. It was difficult to estimate the length of these since they were within the bulk of the porous medium. However, by about $t = 15$ minutes they may have been as long as 5 cm. These instabilities can be seen at the side of the tank in figure 14. After the experiment had finished, the top layer of beads could be removed and the instabilities viewed from above. The regularity in the spacing of the fingers was worthy of note.

Seven experiments were carried out, five in the small tank and two further ones in the larger tank. The experiments covered a range of q from 31 to 201 cm^3 and of ν from 7.2 to 11.4 cm^2 s, where ν was measured as described in § 3. Table 3 presents the values of θ, ν and q for each experiment as well as the constants S_V, S_H and S_t given by (4.7) for $\alpha = 0$ with $g = 981$ cm s^{-2} and $k = 3.1 \times 10^{-5}$ cm^2.

All the raw data for the length of the currrents as functions of time are presented in figure 15. The non-dimensionalized data of X_N as a function of T are presented

https://doi.org/10.1017/S0022112001004700 Published online by Cambridge University Press

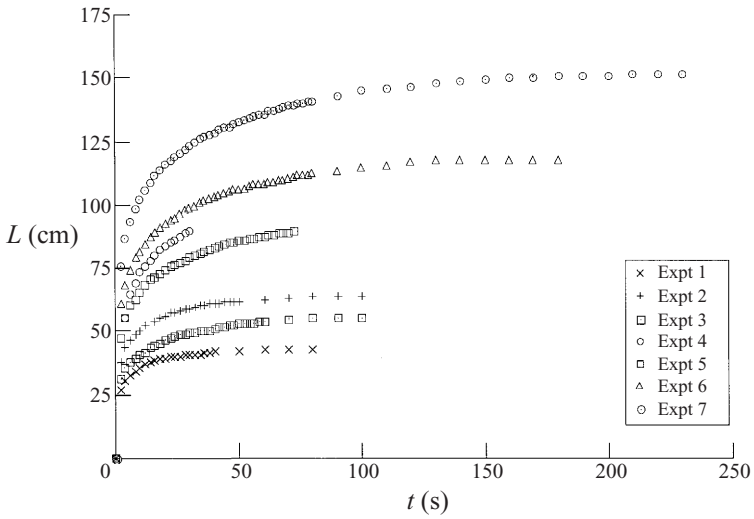


FIGURE 15. The raw data of the positions of the front of the gravity current L as functions of time for the seven experiments described in table 3.

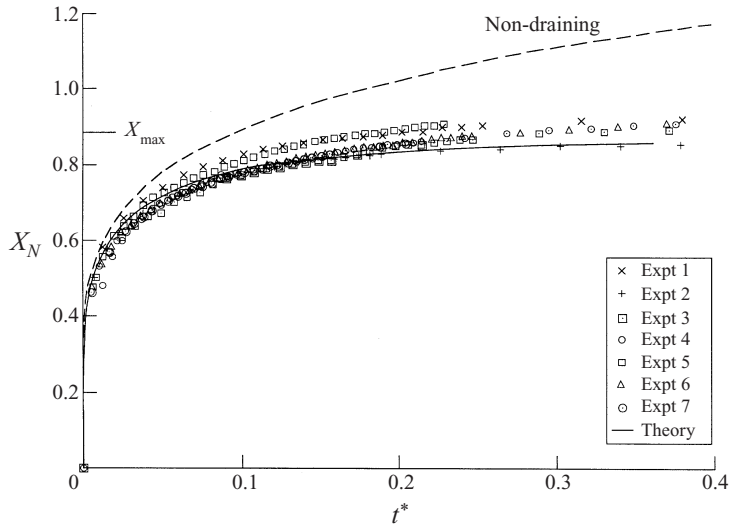


FIGURE 16. The dimensionless extent of the current X_N as a function of dimensionless time for the seven experiments shown in figure 15. The solid curve is the theoretical prediction determined from the numerical integration of (6.2)–(6.5). The dashed curve shows the non-draining similarity solution.

in figure 16, along with the theoretical curve evaluated using the techniques of the previous section. For comparison, the non-draining similarity solution is shown with a dashed curve in figure 16. Unlike the similarity solution, valid for $\alpha = 3$, all the experimental gravity currents and the theoretical prediction, came to rest in finite time. As can be seen, generally the results collapse very well and agree admirably with the theoretical curve. The data all lie above the theoretical curve, much of it within the 5% error estimated in the length of the fringe. A significant error may also have been produced by the fact that the current had covered almost half its

https://doi.org/10.1017/S0022112001004700 Published online by Cambridge University Press

Experiment	θ (°C)	q (cm^2)	v (cm^2 s^{-1})	S_v (cm)	S_H (cm)	S_t (s)
1	23.3	31	7.2	0.67	46.4	158.3
2	21.6	64	9.4	0.85	75.2	263.2
3	20.7	48	9.5	0.77	62.1	241.7
4	22.1	122	9.3	1.06	115.6	322.8
5	21.4	97	9.8	0.98	98.8	314.6
6	22.6	142	8.9	1.11	127.9	325.0
7	22.4	206	9.0	1.26	163.9	372.0

TABLE 3. Parameter values for the seven experiments on draining viscous gravity currents.

final run out while the lock gate was still open. A further source of error may come from the neglect of surface tension in the present theoretical model. Note that the run-out distance would be greater than predicted here if the fluid did not wet the porous medium so that the pressure at the base of the flow were greater than atmospheric and drainage retarded. A quantitative assessment of this awaits further developments of the theory to incorporate surface-tension effects, which is currently being undertaken by Ms Sharon Kahn. In total however, our theoretical concepts and numerical solutions seem to capture the main aspects of the flow in the correct quantitative way.

8. Summary

This paper has presented the results of two related studies. First we examined the one-dimensional drainage of a layer of fluid through a deep porous medium. The pressure field in the fluid layer is governed by the hydrostatic relationship and we used Darcy's equation to model the motion inside the medium. Thus, while the fluid moves downwards everywhere, the total pressure *increases* downwards in the fluid layer and *decreases* downwards in the porous medium. For the situation in which the total volume of fluid remains constant, we showed that at small times the change in height is proportional to $\sqrt{t}$, where t is the elapsed time since the initiation of the experiment. This contrasts with the flow regime at very long times for which the flow velocity is linear. For the situation in which fluid is added to the system at the appropriate rate to ensure that the top of the fluid layer remains fixed, we calculated that the flow rate decays with time to tend to a constant value.

By carrying out a series of experiments in which we allowed glycerine to percolate through a bed of beads we have obtained very strong empirical support for the model. As a by-product, the experimental procedure we developed suggests an easy way to estimate the permeability of a porous medium, especially if its porosity has previously been measured. Our estimates for permeability were consistent between experiments (four experiments allowed us to estimate the permeability to within 3%) and were consistent with the Carman–Kozeny and Rumpf–Gupte empirical relationships for estimating permeabilities. We are confident that this method can easily be extended to measure the permeability of other porous media. This will be especially useful in situations for which no appropriate empirical relationships exist for estimating permeabilities, for example of media in which the constituent particles vary in size and shape.

Second we investigated and considered the flow of a two-dimensional, viscous gravity current propagating over a deep, porous substrate by considering the local

https://doi.org/10.1017/S0022112001004700 Published online by Cambridge University Press

effect on the conservation of fluid due to draining through the porous substrate. When the total volume of the current increases like t^3 (where t is the time since the initiation of the current) the shape of the current is self-similar for all time. In this case the length of the currrent, x_N, is proportional to t^2. The similarity variable evaluated at the position of the nose s_N depends only weakly on the porosity of the bed, varying by only about 20% across a range of 'physically reasonable' porosities. For a porosity of 50% we calculate that $s_N = 0.574$. When the volume of the current increases faster than t^3 it will advance for all time. When the volume increases slower than t^3 the nose of the gravity current will sink below the porous bed and after reaching some maximum length, $x_{\max}$, the front of the fluid above the porous medium will recede. For the case of a release of constant volume q per unit width, we calculate that the total run-out distance is $X_{\max} = (q^4/3k)^{1/6} f(\phi)$ where k is the permeability and $f(\phi)$ is a weak function of the porosity ϕ, having a value of 0.858 at $\phi = 0.37$ and varying by about 30% across the full range of porosities. It is interesting to note that $X_{\max}$ is independent of the viscosity of the fluid, which only influences the rates of flow.

We performed a number of experiments in which we measured the length of a dyed glycerine gravity current flowing over a bed of spherical beads, for the situation in which the total volume is constant. We varied both the viscosity and the volume of the glycerine. The experimental data were in good agreement with the theoretical predictions.

Numerous extensions of the basic concepts presented here are immediately suggested. First, an analysis considering axisymmetric currents could be undertaken. Second, the drainage law will be valid for, and could be applied to, gravity currents propagating at high Reynolds number over a porous bed (into which it drains at low Reynolds number) (Thomas *et al.* 1998 and Ungarish & Huppert 2000). Third, the effects of an initially saturated porous medium could be considered. Fourth, an evaluation of the propagation of a viscous current down a permeable slope could be investigated. Finally, there are numerous natural and industrial situations of fluid flow over porous media.

It is a pleasure to thank Dr M. A. Hallworth for his enthusiastic help and guidance in performing the experiments reported here. We are grateful to J. R. Lister for alerting us to the physical origin of the front condition (4.11*c*) and to R. C. Kerr and M. Ungarish for their helpful comments on an earlier version of the manuscript. This work started as a summer student project for J. M. A, generously supported by a grant from Trinity College, Cambridge.

Appendix. Transformations used in the numerical analysis

The coordinate transformation $Y = X/X_N$ converts (4.8)–(4.10), in the case $\alpha = 0$ to

$$\frac{\partial \eta}{\partial T} - Y\frac{\dot{X}_N}{X_N}\frac{\partial \eta}{\partial Y} - \frac{1}{X_N^2}\frac{\partial}{\partial Y}\left(\eta^3\frac{\partial \eta}{\partial Y}\right) = -\left(\frac{\eta+\zeta}{\zeta}\right), \tag{A 1}$$

$$\frac{\partial \zeta}{\partial T} - Y\frac{\dot{X}_N}{X_N}\frac{\partial \zeta}{\partial Y} = \frac{\eta+\zeta}{\phi\zeta}, \tag{A 2}$$

$$X_N = \frac{1}{V}, \tag{A 3}$$

https://doi.org/10.1017/S0022112001004700 Published online by Cambridge University Press

where

$$V = \int_0^1 (\eta + \phi\zeta)\mathrm{d}Y. \tag{A 4}$$

These are subject to the boundary conditions

$$\eta = \zeta = 0 \quad \text{at} \quad Y = 1, \qquad \frac{\partial \eta}{\partial Y} = 0 \quad \text{at} \quad Y = 0. \tag{A 5}$$

These equations are singular at $Y = 1$, where $\eta \sim (1 - Y)^{1/3}$ and $\zeta \sim (1 - Y)^{2/3}$, cf. (5.9). To eliminate these singularities, we write

$$Y = 1 - u^3 \tag{A 6}$$

whence

$$\frac{\partial \eta}{\partial T} + \left(\frac{1 - u^3}{3u^2}\right)\frac{\dot{X}_N}{X_N}\frac{\partial \eta}{\partial u} - \frac{\eta^3}{9X_N^2 u^4}\frac{\partial^2 \eta}{\partial u^2} + \frac{2\eta^3}{9X_N^2 u^5}\frac{\partial \eta}{\partial u} - \frac{\eta^2}{3X_N^2 u^4}\left(\frac{\partial \eta}{\partial u}\right)^2 = -\left(\frac{\eta + \zeta}{\zeta}\right), \tag{A 7}$$

$$\frac{\partial \zeta}{\partial T} + \left(\frac{1 - u^3}{3u^2}\right)\frac{\dot{X}_N}{X_N}\frac{\partial \zeta}{\partial u} = \frac{\eta + \zeta}{\phi\zeta}, \tag{A 8}$$

$$X_N = \frac{1}{V}, \tag{A 9}$$

where

$$V = 3\int_0^1 (\eta + \phi\zeta)u^2\mathrm{d}u. \tag{A 10}$$

These are subject to boundary conditions

$$\eta = \zeta = 0 \quad \text{at} \quad u = 0, \qquad \frac{\partial \eta}{\partial u} = 0 \quad \text{at} \quad u = 1. \tag{A 11}$$

We used second-order, centered differences for the spatial derivatives and an explicit time step. Although the solutions for η and ζ are analytic in u, some of the coefficients in the equation are singular at $u = 0$, which reduces the order of the numerical scheme and, in fact, introduces errors of $O(1)$. This was overcome by using the asymptotic expressions

$$\eta \sim \eta_1 u + \eta_2 u^2, \quad \zeta \sim \zeta_2 u^2, \tag{A 12a,b}$$

where

$$\eta_1 = (3X_N\dot{X}_N)^{1/3}, \quad \zeta_2 = \left(\frac{3X_N\eta_1}{2\phi\dot{X}_N}\right)^{1/2}, \quad \eta_2 = \frac{3X_N}{8\dot{X}_N}\frac{\eta_1}{l_2}, \tag{A 13a,b,c}$$

to represent the solution between $u = 0$ and $u = (\Delta u)^{1/2}$. The asymptotic expressions are accurate to $O(\Delta u)$ over this range and the numerical scheme has an error of $O(\Delta u)$ over the range $[(\Delta u)^{1/2}, 1]$. Thus, overall, the truncation error is $O(\Delta u)$.

The speed of the boundary $\dot{X}_N$ was calculated in a predictor step by taking the difference between X_N at the current and previous time steps and dividing by Δt. During the corrector step $\dot{X}_N$ was calculated as the difference between X_N at the end of the predictor step and the current step and dividing by Δt.

The scheme was found to converge to three significant figures with a grid spacing of 80 intervals on the range $u \in [0, 1]$.

https://doi.org/10.1017/S0022112001004700 Published online by Cambridge University Press

REFERENCES

Batchelor, G. K. 1967 *An Introduction to Fluid Dynamics*. Cambridge University Press.

Bear, J. 1988 *Dynamics of Fluids in Porous Media*. Dover.

Davis, S. H. & Hocking, L. M. 2000 Spreading and imbibition of viscous liquid on a porous base II. *Phys. Fluids* **12**, 1646–1655.

Delker, T., Pengra, D. B. & Wong, P. 1996 Interface pinning and the dynamics of capillary rise in porous media. *Phys. Rev. Lett.* **76**, 2902–2905.

Dullien, F. A. L. 1979 *Fluid Transport and Pore Structure*. Academic Press.

Huppert, H. E. 1982 The propagation of two-dimensional and axisymmetric viscous gravity currents over a rigid horizontal surface. *J. Fluid Mech.* **121**, 43–58.

Huppert, H. E. 1986 The intrusion of fluid mechanics into geology. *J. Fluid Mech.* **173**, 557–594.

Huppert, H. E. 2000 Geological fluid mechanics. In *Perspectives in Fluid Mechanics – A Collective Introduction to Current Research* (ed. G. K. Batchelor, H. K. Moffatt & M. G. Worster). Cambridge University Press.

Phillips, O. M. 1991 *Flow and Reactions in Permeable Rocks*. Cambridge University Press.

Rumpf, H. & Gupte, A. R. 1971 Einflüsse der porosität und Korngrössenverteilung im Widerstandsgesetz der Poreströmung. *Chem. Ing. Tech.* **43**, 367–375.

Simpson, J. 1997 *Gravity currents in the Environment and the Laboratory*. Cambridge University Press.

Thomas, L. P., Marino, B. M. & Linden, P. F. 1998 Gravity currents over porous substrate. *J. Fluid Mech.* **366**, 239–258.

Ungarish, M. & Huppert, H. E. 2000 Gravity current flows over porous media. *J. Fluid Mech.* **418**, 1–23.

Washburn, E. W. 1921 The dynamics of capillary flow. *Phys. Rev.* **17**, 273–283.

https://doi.org/10.1017/S0022112001004700 Published online by Cambridge University Press